IEEE Access
Multidisciplinary | Rapid Review | Open Access Journal

Received November 5, 2021, accepted November 26, 2021, date of publication November 30, 2021,
date of current version December 22, 2021.

Digital Object Identifier 10.1109/ACCESS.2021.3131868

Efficiency-Improved UWB Transparent Antennas Using ITO/Ag/ITO Multilayer Electrode Films

JEONG-WOOK KIM[1], JU-IK OH[1], KWANG-SEOK KIM[2], JONG-WON YU[1], (Member, IEEE), KANG-JAE JUNG[3], AND IL-NAM CHO[3]

[1]School of Electrical Engineering, Korea Advanced Institute of Science and Technology, Daejeon 34141, Republic of Korea
[2]Affiliated Research Organization of the Electronics and Telecommunications Research Institute, Daejeon 34044, South Korea
[3]Advanced Standard Research and Development Laboratory, LG Electronics Inc., Seoul 150721, Republic of Korea

Corresponding author: Kwang-Seok Kim (kks21ckr@nsr.re.kr)

ABSTRACT In this paper, a transparent antenna made with a new structure of ITO/Ag/ITO is proposed. Overcoming the physical limitations of transparency and conductivity is an important problem with transparent materials. By studying and comparing previously reported transparent materials, a transparent electrode with thin film Ag inserted between two layers of ITO instead of a single layer is selected for a highly efficient transparent antenna. This electrode has low sheet resistance (3.1 Ω/sq) relative to its high transparency (88 % at 550 nm), which is a factor that can increase the efficiency of the antenna. In general, it is difficult to measure sheet resistance (SR) using a 4-point DC probe for very thin films (thickness of transparent material is less than the skin-depth). Therefore, a form of reverse engineering that can estimate DC sheet resistance using RF SR was presented and verified. As a result, it was possible to predict and design the performance of the transparent antenna with the new material structure. The selected transparent material is applied to design the wideband transparent antenna and the design process for wideband performance is covered in the paper. The proposed antenna with ITO/Ag/ITO was implemented for verification. The peak efficiency of the fabricated antenna was 66 %, and the measured bandwidth was 123 % (from 2.5 GHz to 10.6 GHz), which is the best performance than previously reported transparent antennas.

INDEX TERMS Transparent antenna, efficiency improvement, ultra-wideband, ITO/Ag/ITO films.

I. INTRODUCTION

Recently, transparent antennas for use in various applications such as electronics products, mobile phones, and vehicle communication are being studied [1]. In these applications, a wideband high efficiency antenna is essential for improved communication. Moreover, to use a transparent antenna, high transparency over 85 % is required [2]. The issue is the trade-off between the conductivity and transparency in transparent electrodes. In other words, the better the optical transparency is, the lower the electrical conductivity becomes. Therefore, many studies have been conducted to overcome this.

Transparent antennas have been studied using a variety of transparent materials [3]–[31]. There are two approaches to design a transparent antenna. One is to use oxide-based transparent material. Of these, indium tin oxide (ITO) is the most common material for transparent electrodes [3]–[7]. This ITO has transparency (81 - 85 %) and high sheet resistance (SR, 7 - 10 Ω/sq), resulting in low antenna efficiency.

To overcome the high sheet resistance, indium tin oxide with Ag or Au thin films are applied to the transparent antenna [8]–[10]. In [8], the transparent coplanar waveguide (CPW)-fed monopole antenna has high transparency (85 %), and the peak antenna efficiency is 70 %. In addition, the fractional bandwidth is 155.6 %, which is suitable for a wideband transparent antenna. However, the shape of the antenna is visible because it uses gold nanolayer deposition. In [9], [10], AgITO is used for a transparent slot antenna. This material has low sheet resistance (0.9 Ω/sq). Because of the low sheet resistance, the antenna has high peak efficiency (71 - 80 %), but the transparency is too low (52.5 %). Moreoever, the slot antenna has limited fractional bandwidth, and the double layer for the feeding network makes the transparency lower.

Fluorine tin oxide (FTO) transparent electrodes and fluorine-doped tin oxide/indium tin oxide (FTO/ITO) have been studied for improved transparency and sheet

The associate editor coordinating the review of this manuscript and approving it for publication was Davide Ramaccia.

This work is licensed under a Creative Commons Attribution 4.0 License. For more information, see https://creativecommons.org/licenses/by/4.0/

resistance [11], [12]. In [11], FTO has sheet resistance (9 Ω/sq) and transparency (80 %) similar to that of ITO. FTO/ITO has low sheet resistance (4 Ω/sq), which leads to the high peak efficiency (60 %). Moreover, the monopole type antennas have wide fractional bandwidth (128 %). However, their transparency is too low (72 %), and as with the antenna in [9], [10], the double layer makes the feeding network visible.

Another approach is to employ metal for the transparent antenna. AgHT is a thin Ag films that has transparency (80 - 85 %) and high sheet resistance (8 Ω/sq) [13]–[19]. Moreover, the dual-band antennas in [14]–[17] are not suitable for a wideband application. In [18], a transparent CPW-fed slot antenna with high peak efficiency (80 %) is researched. However, the transparency is too low (80 %), and the fractional bandwidth is too narrow (40 %). Mesh metal and nanohole structures have also been studied for use in transparent antennas [20]–[24]. These materials have low sheet resistance and high transparency. However, the high optical haze resulting from scattering of the nanowires and mesh patterns is undesired in high-resolution displays [25]. Moreover, they are usually fabricated through precise patterning or complicated chemical synthesis processes which makes fabrication procedures expensive and complex [26], [27].

To overcome the problems with conventional transparent materials, multilayer electrode films are used for transparent antennas [28]–[32]. Structures like this are sealed with bottom and top oxide films, which act as suitable barriers against chemical corrosion of the metals [33]. In [28], IZTO (40 nm)/Ag (10 nm) /IZTO (40 nm) is used for a transparent antenna. It has high transparency (86 %), but the sheet resistance (7 Ω/sq) is too high. The transparent antenna has a narrow fractional bandwidth (40 %) and is not suitable for a wideband application. In [29]–[31] IZTO (45 nm)/Ag (10 nm) /IZTO (45 nm) is employed. It has low sheet resistance of 2.52 Ω/sq [30], [31]. In [32], a monopole-type antenna operates over a wide fractional bandwidth (109 %), but the antenna efficiency (42.1 %), and transparency (80 %) are both low. Moreover, ITO (85 nm)/Ag (13 nm)/ITO (85 nm) has low transparency (74 %) and high sheet resistance (5 %). To design a transparent antenna that has over 85 % transparency, high antenna efficiency, and a broad operating bandwidth, a new material, and proper antenna structure had to be researched.

In this paper, a new multilayered transparent antenna using the best transparent material is proposed to improve electrical performance while maintaining a high transparency state. We selected the best transparent material for a highly efficient transparent, wideband antenna. To implement it, we applied this material to create a CPW-fed diamond-shaped monopole antenna. Moreover, to design the transparent antenna using the new transparent material, reverse engineering was used to estimate the electrical property of the selected material, which result is presented. To design a transparent antenna with the new material, it is necessary to know the RF sheet resistance

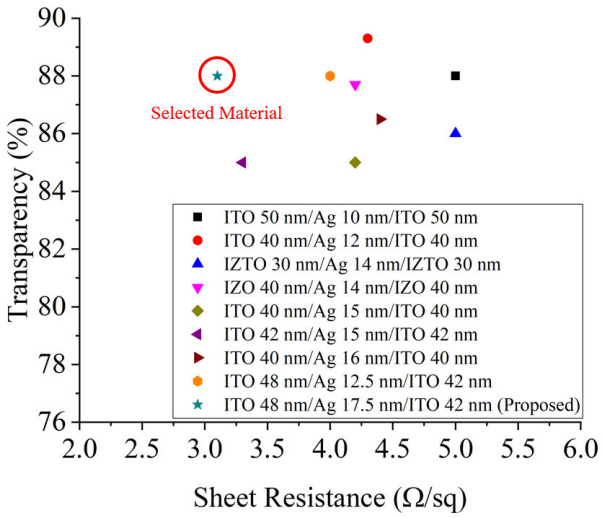

FIGURE 1. The transparent materials reviewed for selecting the best transparent material.

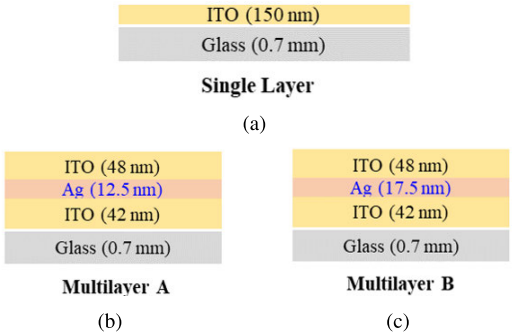

FIGURE 2. The designed transparent material layer information of (a) Single layer (SL), (b) Multilayer A (MA), and (C) Multilayer B (MB).

of the transparent material. Traditionally, the DC sheet resistance is employed in place of the RF sheet resistance because, for thin films (thickness of transparent material less than skin-depth), RF and DC SR are the same [34]. However, measuring the sheet resistance requires a 4-point DC probe that costs more and takes more time. Moreover, damage occurs to the thin film sample due to the pressure from physical contact [35], [36]. Therefore, in Section II, we introduce for the first time, a method for predicting DC SR using RF SR by reverse engineering. In Section III, the design of the proposed transparent antenna made using the selected transparent material is covered. In Section IV, the implementation of the proposed antenna structure is verified. Section V presents conclusions about the proposed antenna.

II. TRANSPARENT MATERIAL DESIGN

A. TRANSPARENCY PROPERTY

To design a transparent antenna, first, an appropriate transparent material is needed. To select the transparent material, we investigated a transparent material with transparency > 85 % [37]–[44]. As shown in Fig. 1, an ITO (48 nm)/Ag

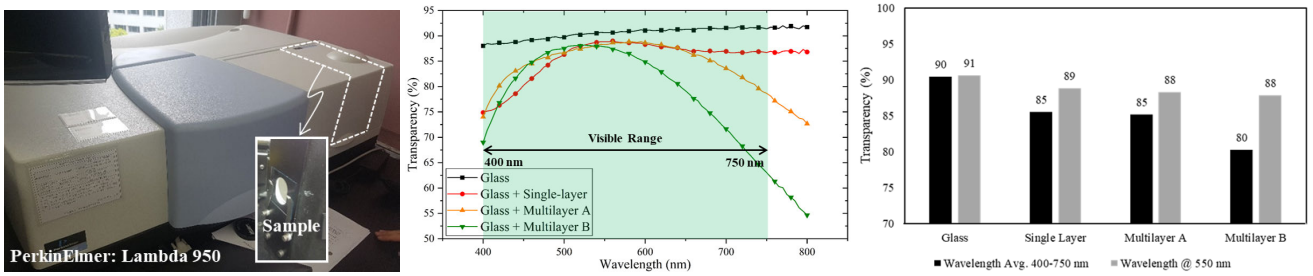

(a) (b) (c)

FIGURE 3. **(a) The optical characteristic measurement environment, (b) the measured transparency results of transparent materials according to wavelength, and (c) the measured transparency of transparent materials in the average visible range and at 550 nm.**

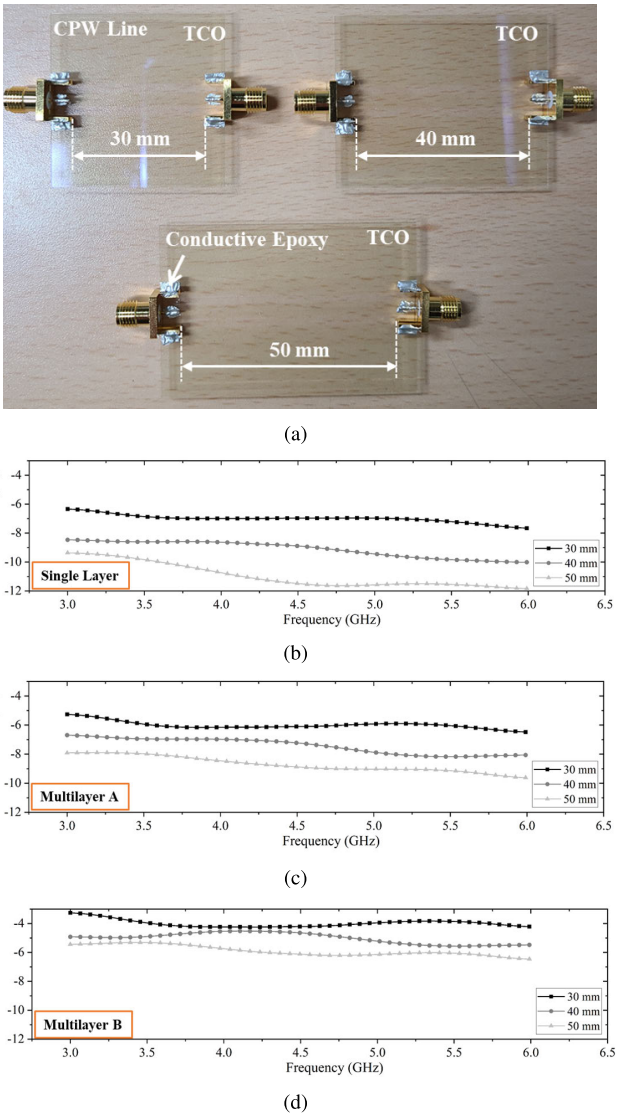

(a) (b) (c) (d)

FIGURE 4. **(a) The fabricated CPW transmission line using transparent material to predict RF characteristics of the sheet resistance (SR). The measured results of insertion loss for (b) SL, (c) MA, and (d) MB.**

(17 nm)/ITO (42 nm) material has the lowest sheet resistance (3 Ω/sq) and its transparency is 88 %. This material satisfies the need for > 85 % transparency and low sheet resistance can make the antenna efficiency high.

TABLE 1. **Comparisons of the measured delta insertion loss.**

	SL	MA	MB
$S_{21(30mm)} - S_{21(40mm)}$ (dB/mm)	0.21	0.14	0.10
$S_{21(40mm)} - S_{21(50mm)}$ (dB/mm)	0.19	0.13	0.09
$S_{21(30mm)} - S_{21(50mm)}$ (dB/mm)	0.20	0.13	0.09
Avg. (dB/mm)	0.20	0.13	0.09

To compare with other materials, three transparent electrodes were designed, as shown in Fig. 3. The electrodes were implemented using RF magnetron sputtering [44]. There were three configurations: Single-layer ITO (150 nm), "Multilayer A" ITO/Ag/ITO (48/12.5/42 nm), and "Multilayer B" ITO/Ag/ITO (48/17.5/42 nm). Corning glass with a relative permittivity of 5.27, loss tangent of 0.001, and thickness of 0.7 mm was used for the substrate. From an optical point of view, the wavelengths 400-750 nm encompass the visible range. In particular, light at 550 nm is that to which the human eye is most sensitive [45]. As shown in Fig. 3(a), the transparency was measured using a PerkinElmer' Lambda 950. The transparency to visible light of the new transparent electrode is shown in Fig. 3(b). In Fig. 3(c), the ITO single-layer (SL) and multilayer A (MA) were higher in terms of the 400-750 nm average transparency. At 550 nm, the single-layer, MA, and multilayer B (MB) showed similar transparency (1 % difference). The optical characteristics at 400-750 nm were analyzed. The SR characteristics were analyzed based on the RF property as an electrical analysis method.

B. REVERSE ENGINEERING TO DETERMINE THE ELECTRICAL PROPERTY

In general, the conductivity of a transparent electrodes cannot be known given the new structure of the material. A 4-point probe measurement analyzes the DC SR of the electrical characteristics. However, for very thin films, it is difficult to measure sheet resistance using a 4-point DC probe [35], [36]. Because the layer is so thin, the measurement error due to the DC probe contact is very large. If an electrode with thickness less than the skin-depth, is used in the operating frequency range, RF SR verification is possible using the following equation [34].

$$R_S^{DC} = \frac{1}{\sigma_{Films} t_{Films}} \tag{1}$$

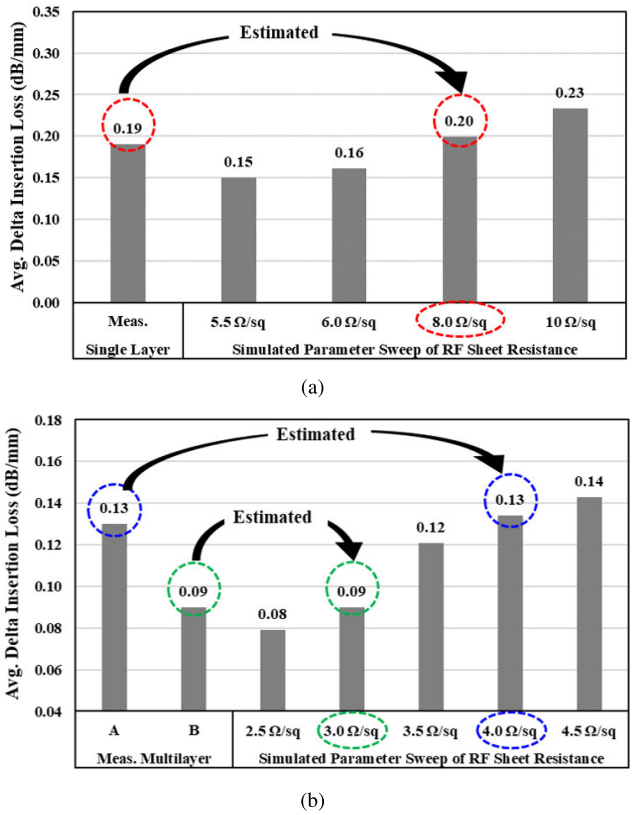

FIGURE 5. Estimation for delta insertion loss according to RF SR of (a) SL, and (b) MA, and MB.

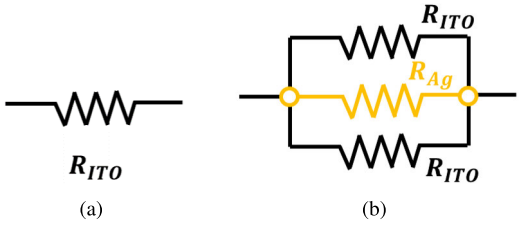

FIGURE 6. Equivalent circuit of (a) single layer and (b) multilayer.

$$R_S^{RF} = \frac{1}{\sigma_{Films}\delta_{Films}}\left(where: \delta_{Films} = \sqrt{\frac{2}{\omega\mu_0\sigma_{Films}}}\right) \cong \frac{1}{\sigma_{Films}t_{Films}}\left(when: t_{Films} \ll \delta_{Films}\right) \quad (2)$$

$$\therefore R_{S,Films}^{DC} \cong R_{S,Films}^{RF} \quad (3)$$

Equation (1) is the formula of SR ($R_{\square}^{DC}$) with conductivity (σ_{Films}). The thickness (t_{Films}) here can be seen as the effective thickness in terms of DC. However, in RF, skin-depth (δ_{Films}) occurs depending on the frequency (ω). Thus, equation (1) should be represented, including skin-depth, as shown in (2). In equations (1) and (2), the conductivity (σ_{Films}) is lower because the carrier concentration and hall mobility are low due to the thin metal and not bulky [46]. In the case of the thin film (1xx nm), the thickness of the transparent material is less than the skin-depth; so the RF and DC SR are equal in the UWB band as seen in equation (3) [34]. Therefore, in a thin-film material (1xx nm), the DC SR can be obtained by reverse engineering.

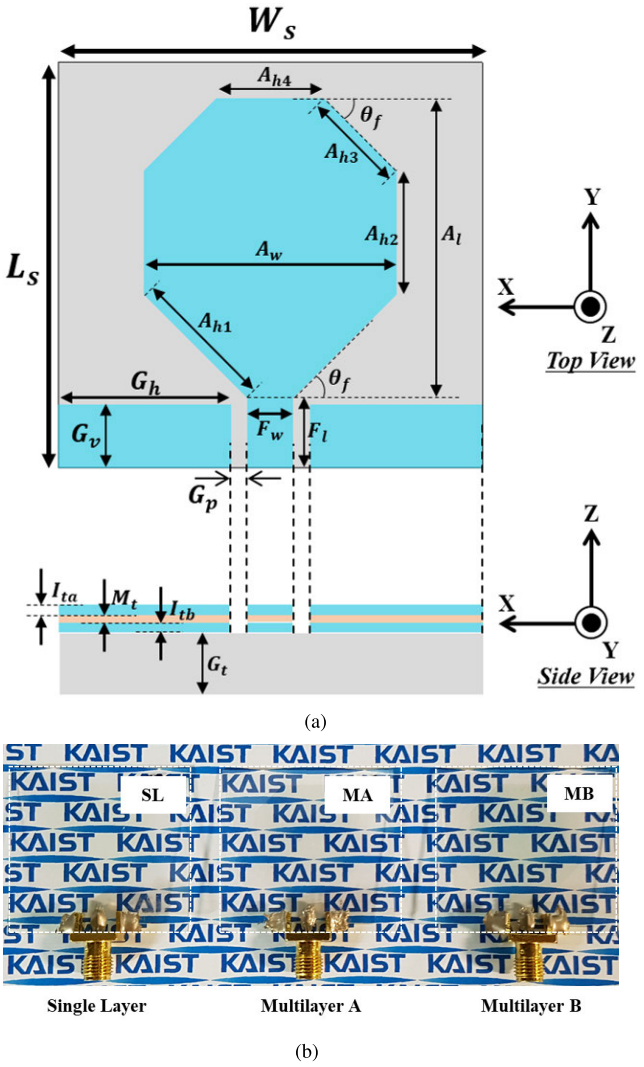

FIGURE 7. (a) Geometry of the proposed transparent antenna with $W_s = 36.6$, $L_s = 35$, $A_l = 26$, $A_w = 22$, $A_{h4} = 9.3$, $A_{h3} = 8.8$, $A_{h2} = 11$, $A_{h1} = 12.6$, $G_h = 15$, $G_v = 5.5$, $G_p = 1.4$, $G_t = 0.7$, $F_w = 4$, $F_l = 6$ (in millimeters), $I_{ta} = 48$, $M_t = 17.5$, $I_{tb} = 42$ (in nanometers), $\theta_f = 45°$. (b) Implementation of the proposed transparent antennas.

First, for when the conductivity of a transparent material cannot be known, the transmission lines of CPW using SL, MA, and MB were fabricated to analyze the RF SR characteristics for reverse engineering. The insertion loss per unit length for each transparent material was measured. Fig. 4(a) shows the fabricated CPW of the transmission line with the transparent materials (i.e., 30, 40, and 50 mm). Fig. 4(b)-(d) shows the insertion loss for the SL, MA, and MB. The loss factor for each frequency improves in the order SL, MA, and MB. As shown in Fig. 4(b)-(d), based on the insertion loss, it can be expressed as a representative value of the average insertion loss per unit length (3-6 GHz), as summarized in Table 1.

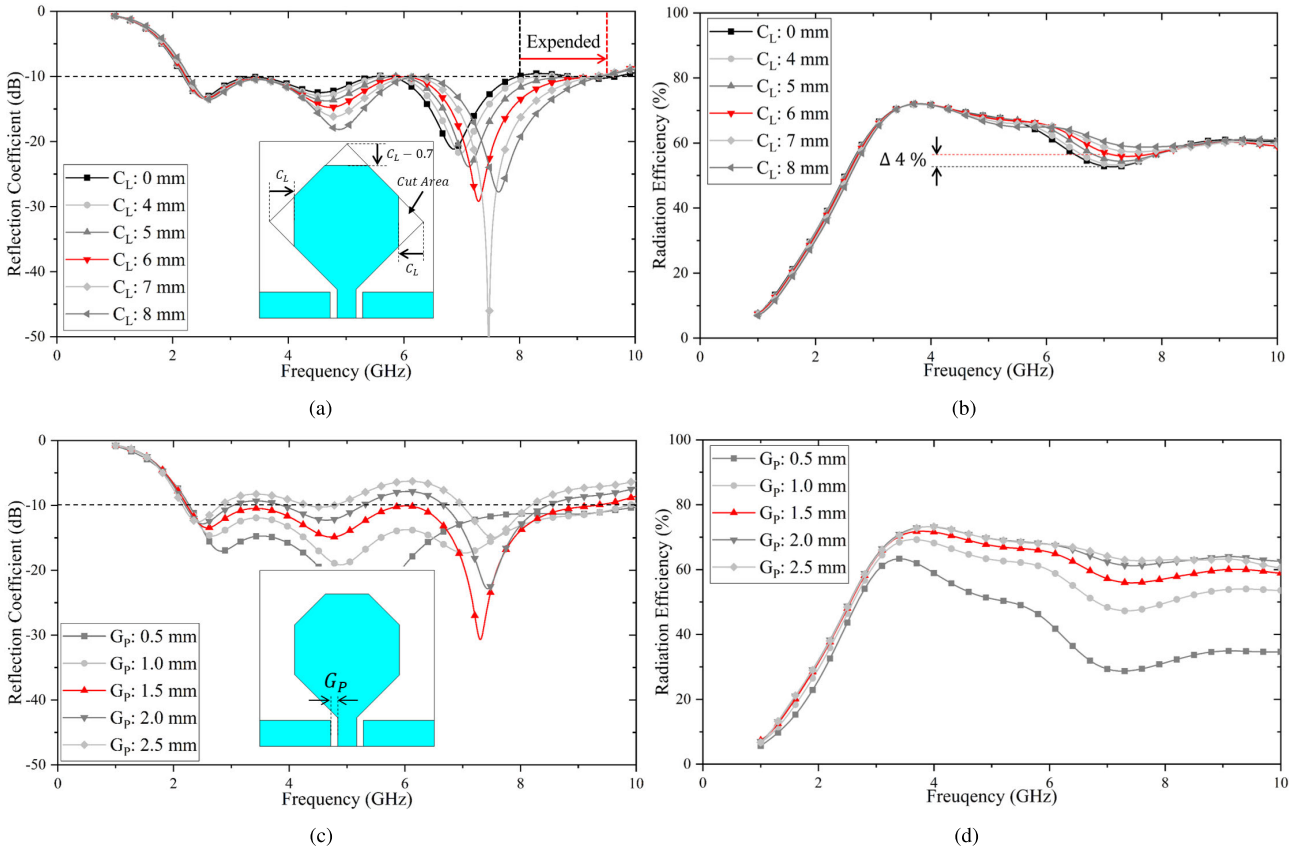

FIGURE 8. Variations in the reflection coefficient and radiation efficiency according to (a)-(b) Cutting area and (c)-(d) Gap between feeder and ground.

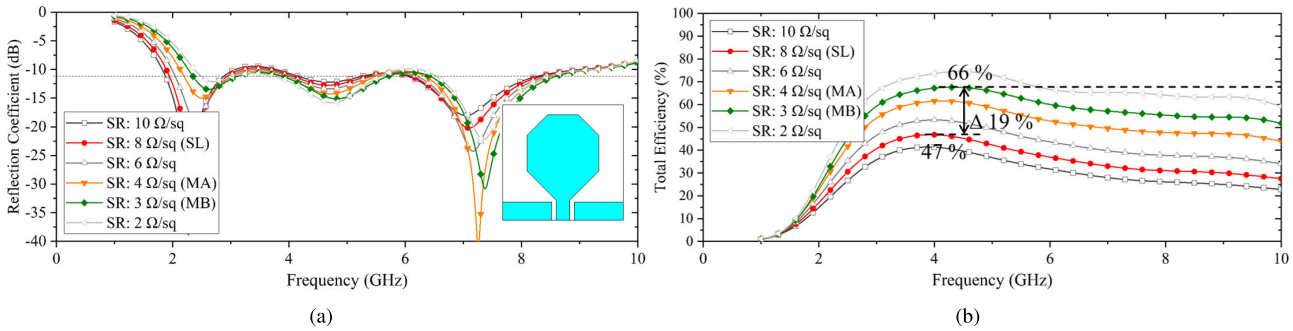

FIGURE 9. Variations according to SR: (a) Reflection coefficient and (b) Total efficiency.

The average delta insertion loss (ADIL) per unit length is 0.2 dB/mm for SL, 0.13 dB/mm for MA, and 0.09 dB/mm for MB. Based on the measured ADIL, a 3-D electromagnetic (EM) simulator was set up to estimate RF SR as being in the same environment as the CPW transmission line manufactured. Then, the same ADIL could be extracted by the sweep of the SR parameter of the transparent material. Fig. 5(a) shows that the RF SR estimated with the measured ADIL is 8 Ω/sq as a result of variation of the SR to 5.5-10 Ω/sq for the SL. Similarly, Fig. 5(b) shows that the estimated SRs of MA and MB are 4 Ω/sq and 3 Ω/sq, respectively. As such, a multilayer may have higher conductivity than a single layer, which is illustrated by equalizing materials that may be configured in parallel, as shown in Fig. 6, where $R_{total}^{SL} = R_{ITO}$ and $R_{total}^{ML} = R_{ITO} \| R_{Ag} \| R_{ITO}$. In this case, since R_{total}^{ML} is constructed in a parallel relationship, conductivity can be improved. The measured DC SRs of SL, MA, and MB were 8.4, 4.3, and 3.1 Ω/sq, respectively. Thus, the RF SR can be equal to DC SR and the factor for predicting the efficiency in antenna design, as described in Section III. By reverse engineering, DC SR was estimated from the RF SR. Moreover, the selected MB

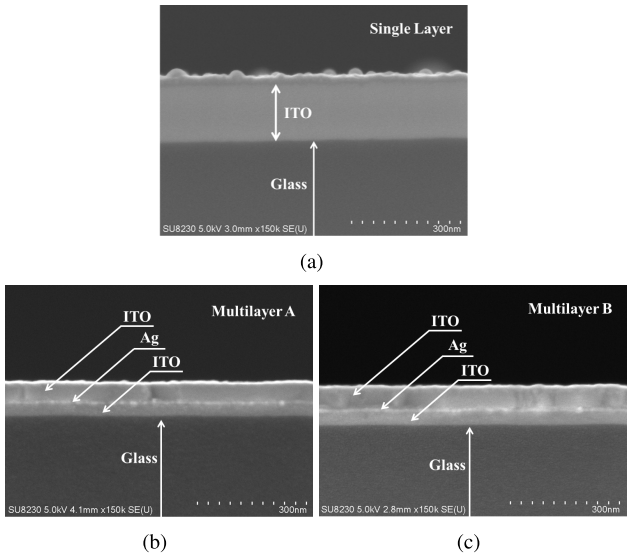

FIGURE 10. Scanning electron microscope (SEM) image with backscattered electrons for (a) SL, (b) MA, and (c) MB.

had the lowest sheet resistance among the three transparent materials.

III. TRANSPARENT ANTENNA DESIGN

To design a wideband, highly efficient transparent antenna using the selected transparent material, a diamond-shaped monopole antenna was designed, as shown in Fig. 7. The proposed transparent antenna was designed using SL, MA, and MB. For high transparency, the transparent antenna had to be designed as a single layer antenna. Moreover, for wideband application, the printed monopole antenna was suitable. Therefore, a CPW-fed monopole antenna was designed.

Fig. 8 shows the reflection coefficient and efficiency according to the C_L and G_P for the essential parameters in terms of antenna design when the SR is 3 Ω/sq (MB). Fig. 8(a) shows the reflection coefficient for the process of becoming antenna C by adding the cutting area (CA) in the rhombus shape. When the CA length (C_L) is increased from 0 to 8 mm, it can be seen that the 10 dB IBW expands to the 9 GHz band. The upper C_L is 0.7 mm less than the C_L on both sides, which is a factor that can increase IBW by asymmetric current induction. The IBW is largest when the C_L is 6 mm. As shown in Fig. 8(b), the efficiency increases by 4 % in the 7.1 GHz band when the C_L is 6 mm rather than 0 mm, so the C_L is most optimal at 6 mm. Fig. 8(c) and (d) show the results of the reflection coefficient and efficiency according to the gap change between the feeder line and ground. As shown in Fig. 8(c), the antenna is improved in terms of the IBW and the impedance matching when G_P is 0.5 mm, 1.0 mm, and 1.5 mm. However, in Fig. 8(d), the efficiency is optimal when G_P is 1.5 mm.

Fig. 9 illustrates variations in the reflection coefficient and efficiency according to the SR of the antennas. The thickness of the ITO and Ag layers could be changed in the process of

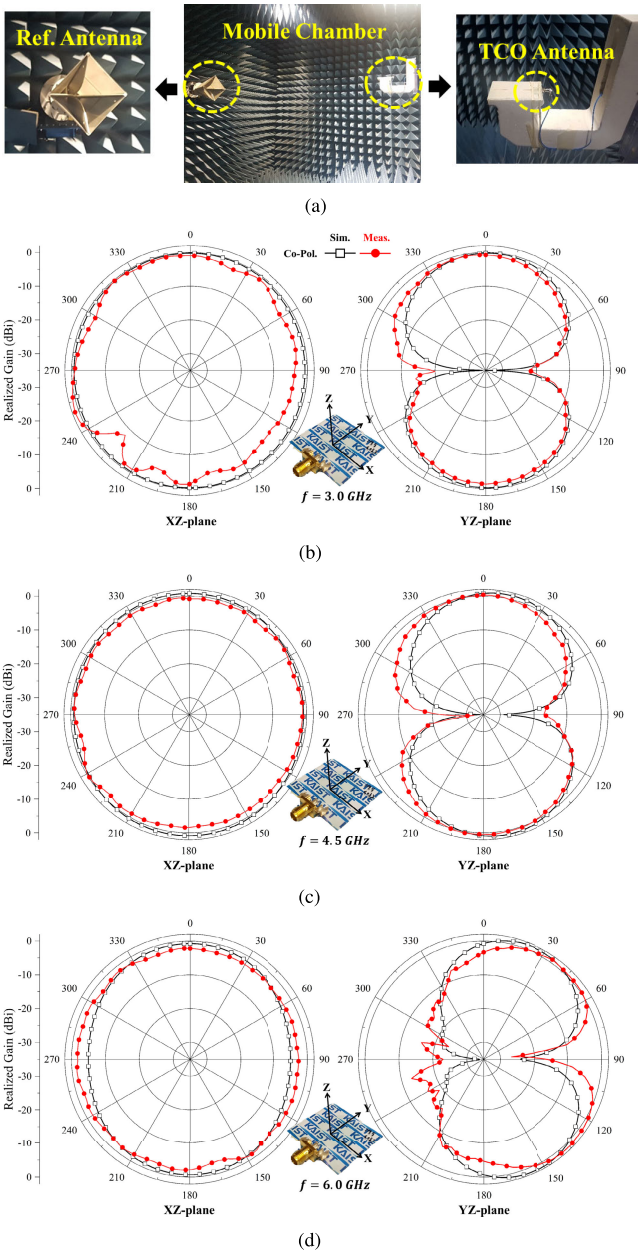

FIGURE 11. (a) The mobile chamber environment for efficiency measurement. Simulated and measured radiation patterns of the proposed antenna at (b) 3.0 GHz, (c) 4.5 GHz, and (d) 6.0 GHz in the XZ and YZ planes.

implementation. In this case, the sheet resistance becomes different. In Fig. 9 (a), the bandwidth in the lower frequency band of the reflection coefficient becomes narrow as the sheet resistance decreases. However, the high frequency performance is maintained as the sheet resistance is varied. Moreover, as the sheet resistance decreases, the antenna efficiency increases. The difference in the peak efficiency between SL and MB is 19 %. Although the peak efficiency is different, the proposed antenna has similar tendencies regarding the reflection coefficient and efficiency according to change in the SR. This is an advantage in terms of reducing a process error when depositing a transparent electrode.

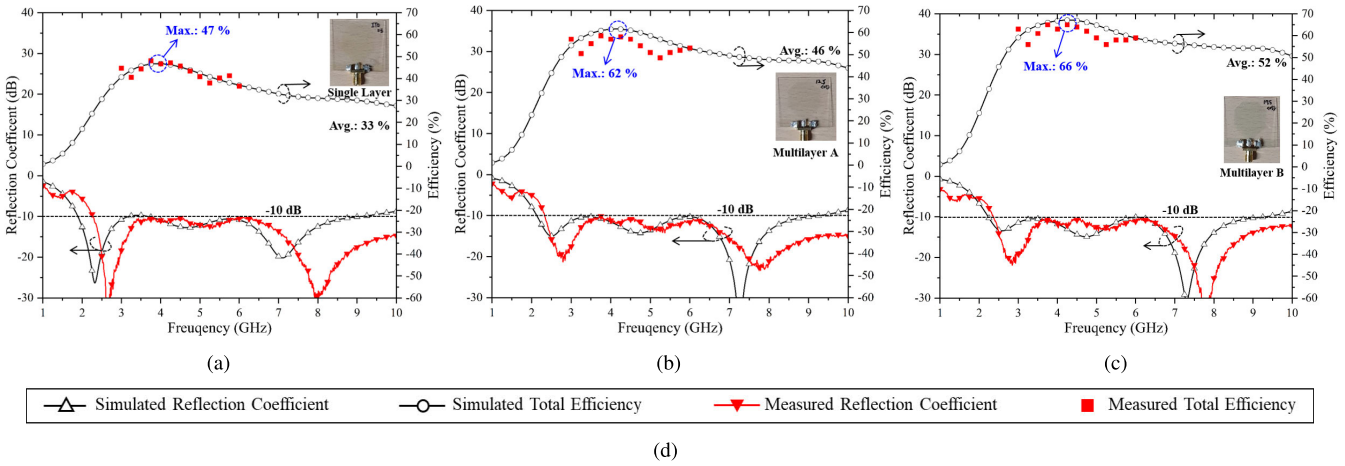

FIGURE 12. The simulated and measured reflection coefficient of the implemented antenna with transparent materials and efficiency: (a) SL, (b) MA, (c) MB, and (d) Caption.

TABLE 2. Comparison with the previously reported high performance transparent antennas.

Reference	Material	Antenna Type	Impedance Bandwidth (%)	Sheet Resistance (Ω/sq)	Peak Efficiency (%) (@ Frequency)	Transparency (%)
2021 [9]	AgITO	Slot	106	0.9	70 (5.8 GHz)	52.5
2021 [12]	FTO/ITO	UWB	128	4.0	60 (7 GHz)	72
2015 [28]	IZTO 40 nm/Ag 10 nm/IZTO 40 nm	Branch	40	7.0	54 (1.54 GHz)	86
2016 [29]	IZTO 45 nm/Ag 10 nm/IZTO 45 nm	Monopole	-	2.5	46.3 (@ 2.45 GHz)	81
2016 [31]	IZTO 45 nm/Ag 10 nm/IZTO 45 nm	Monopole	109	2.5	42 (@ 6.5 GHz)	80
This Work (SL)	ITO 150 nm	CPW-Fed Monopole	130	8.4	58 (3.9 GHz)	89
This Work (MA)	ITO 48 nm /Ag 12.5 nm /ITO 42 nm	CPW-Fed Monopole	124	4.8	64 (4.3 GHz)	88
This Work (MB)	ITO 48 nm /Ag 17.5 nm /ITO 42 nm	CPW-Fed Monopole	123	3.1	66 (4.5 GHz)	88

IV. IMPLEMENTATION AND MEASUREMENT

Diamond-shaped antennas with SL, MA, and MB were implemented, as shown in Fig.8(a). The transparent antennas clearly show the logo on the back of the antenna, as shown in Fig. 8(b). The shape of the antenna is difficult to distinguish with the human eye. Fig. 10 shows a scanning electron microscope image made with backscattered electrons to capture the nanoscale tomography of the three transparent materials. Fig. 10(a) shows the layer composition for the single-layer ITO. Measurements show that the ITO was deposited at a thickness of about 155 nm, showing a process error of about 3 %. As shown in Fig. 10(b), MA was deposited using RF sputtering as ITO/Ag/ITO films with 47.4/13.8/42 nm from the top. It can be seen that the layers are distinguishable. Moreover, Fig. 10(c) is a cross-sectional photograph of MB, in which an increase can be seen compared to the Ag layer of the MA (about 48.6/16.5/44). This could lead to improved electrical properties. As a result, although there is a process error, the multilayer has little optical deteriorations due to the nanoscale layer in the middle, while the sheet resistance is reduced compared to the single layer.

As shown in Fig. 11(a), the 3-D radiation patterns of the proposed transparent antennas were measured in a mobile chamber. A dual-polarized horn antenna was employed as a reference antenna (LB-780-SF). As a result of measurement, it was determined that the radiation patterns of the proposed transparent antenna simulated and measured at the XZ and YZ plane at each frequency (3.0, 4.5, and 6.0 GHz), each show good agreement.

Fig. 12 shows the measured reflection coefficient and efficiency for newly fabricated antennas: diamond shaped monopole antennas with an SL, MA, and MB. The chamber able to measure the antenna efficiency is for mobile use, which means that the frequency band can be measured is only available up to 6 GHz. Therefore, only 3 - 6 GHz was measured considering the sweep point. The measured impedance (whole band) and efficiency (3-6 GHz) of all antennas are in good agreement with simulated results. Therefore, in the band where the efficiency was not measured, the efficiency could be predicted to correspond to the simulated results. The implemented antennas have wider impedance bandwidth than the simulated results do. The maximum efficiencies of the SL, MA, and MB antenna are 47, 62, and 67 %, respectively.

Table 2 summarizes the performance of previously reported transparent antennas. In [9], an AgITO based slot antenna has wide impedance bandwidth (106 %) and high peak efficiency (70 %) due to low sheet resistance (0.9 Ω/sq). However, the transparency is too low (52.5 %). In [12], the UWB antenna with wide bandwidth performance (128 %) studied has peak efficiency that is high enough (60 %). Unfortunately, the transparency is too low (72 %). In [28], [29], and [31], IZTO/Ag/IZTO is employed for transparent antennas. The transparent antenna in [28] was designed using IZTO 40 nm/Ag 10 nm/IZTO 40nm. The

branch-type antenna has a narrow bandwidth. Moreover, in [29] and [31], a monopole antenna with IZTO 45 nm/Ag 10 nm/IZTO 45 nm was studied. This material has a low sheet resistance of 2.5 Ω/sq. However, the proposed transparent antenna efficiency is higher than conventional antennas [29], [31]. Among the previously reported transparent antennas and new transparent antennas in this paper, the proposed transparent antenna using ITO 48 nm /Ag 17.5 nm /ITO 42 nm has high antenna efficiency, broad impedance bandwidth, and proper transparency.

V. CONCLUSION

In this paper, a new diamond-shaped antenna with ITO/Ag/ITO structure was proposed to overcome existing optical and electrical limitations. In the middle, rather than a single layer, Ag was thinly deposited at nanoscale to maximize conductivity performance without deterioration of the transparency. Moreover, for the new material, a reverse engineering method was proposed to overcome the limits of a method that made it difficult to measure thin films using the sheet resistance analysis method. A transparent antenna designed with DC SR estimated using reverse engineering was verified. As a result, it was possible to predict the DC SR of the thin film of the new material and design the antenna. Therefore, it has been verified that the transparent antenna using ITO/Ag/ITO is superior to other materials in terms of efficiency. In addition, the improved efficiency and widened IBW of the proposed antenna was verified by adding a cutting area in the conventional rhombus shape. The proposed antenna has high transparency, high efficiency, and broad wideband performance.

REFERENCES

[1] S. Y. Lee, M. Choo, S. Jung, and W. Hong, "Optically transparent nano-patterned antennas: A review and future directions," *Appl. Sci.*, vol. 8, no. 6, p. 901, 2018.

[2] S. Y. Lee, D. Choi, Y. Youn, and W. Hong, "Electrical characterization of highly efficient, optically transparent nanometers-thick unit cells for antenna-on-display applications," in *IEEE MTT-S Int. Microw. Symp. Dig.*, Jun. 2018, pp. 1043–1045.

[3] Y. Yao, W. Chen, X. Chen, and J. Yu, "Design of optically transparent antenna with directional radiation patterns," *Int. J. Antennas Propag.*, vol. 2017, pp. 1–7, Aug. 2017.

[4] C. White and H. R. Khaleel, "Flexible optically transparent antennas," *WIT Trans. State-Art Sci. Eng.*, vol. 82, p. 59, Oct. 2014.

[5] J. I. Trujillo-Flores, R. Torrealba-Meléndez, J. M. Muñoz-Pacheco, M. A. Vásquez-Agustín, E. I. Tamariz-Flores, E. Colín-Beltrán, and M. López-López, "CPW-fed transparent antenna for vehicle communications," *Appl. Sci.*, vol. 10, no. 17, p. 6001, Aug. 2020.

[6] M. D. Poliks, Y.-L. Sung, J. Lombardi, R. Malay, J. Dederick, C. R. Westgate, M.-H. Huang, S. Garner, S. Pollard, and C. Daly, "Transparent antennas for wireless systems based on patterned indium tin oxide and flexible glass," in *Proc. IEEE 67th Electron. Compon. Technol. Conf. (ECTC)*, May 2017, pp. 1443–1448.

[7] F. Lopez-Marcos, R. Torrealba-Melendez, M. A. Vasquez-Agustin, J. M. Munoz-Pacheco, and E. I. Tamariz-Flores, "A fractal octagonal-shaped transparent antenna for C-band applications," in *Proc. 17th Int. Conf. Electr. Eng., Comput. Sci. Automat. Control (CCE)*, Nov. 2020, pp. 1–5.

[8] R. H. Mohammad, N. M. Mohammad, A. L. N. Abbas, and N. Alireza, "Improving the efficiency of transparent antenna using gold nanolayer deposition," *IEEE Antennas Wireless Propag. Lett.*, vol. 15, pp. 4–7, 2016.

[9] N. A. Eltresy, A. E. M. A. Elhamid, D. M. Elsheakh, H. M. Elhennawy, and E. A. Abdallah, "Silver sandwiched ITO based transparent antenna array for RF energy harvesting in 5G mid-range of frequencies," *IEEE Access*, vol. 9, pp. 49476–49486, 2021.

[10] N. A. Eltresy, A. M. A. Elhamid, D. N. Elsheakh, E. A. Abdallah, and H. M. Elhennawy, "AgITO for high-performance semi-transparent wide-band antenna applications," *Electron. Lett.*, vol. 56, no. 15, pp. 749–750, Jul. 2020.

[11] D. Potti, G. N. A. Mohammed, K. Savarimuthu, S. Narendhiran, and G. Rajamanickam, "An ultra-wideband rectenna using optically transparent vivaldi antenna for radio frequency energy harvesting," *Int. J. RF Microw. Comput.-Aided Eng.*, vol. 30, no. 10, p. e22362, Oct. 2020.

[12] D. Potti, Y. Tusharika, M. G. N. Alsath, S. Kirubaveni, M. Kanagasabai, R. Sankararajan, S. Narendhiran, and P. B. Bhargav, "A novel optically transparent UWB antenna for automotive MIMO communications," *IEEE Trans. Antennas Propag.*, vol. 69, no. 7, pp. 3821–3828, Jul. 2021.

[13] S. Hakimi, S. K. A. Rahim, M. Abedian, S. M. Noghabaei, and M. Khalily, "CPW-fed transparent antenna for extended ultrawideband applications," *IEEE Antennas Wireless Propag. Lett.*, vol. 13, pp. 1251–1254, 2014.

[14] M. A. Malek, S. Hakimi, S. K. A. Rahim, and A. K. Evizal, "Dual-band CPW-fed transparent antenna for active RFID tags," *IEEE Antennas Wireless Propag. Lett.*, vol. 14, pp. 919–922, 2014.

[15] A. Desai, C. D. Bui, J. Patel, T. Upadhyaya, G. Byun, and T. K. Nguyen, "Compact wideband four element optically transparent MIMO antenna for mm-wave 5G applications," *IEEE Access*, vol. 8, pp. 194206–194217, 2020.

[16] A. Desai, T. Upadhyaya, M. Palandoken, J. Patel, and R. Patel, "Transparent conductive oxide-based multiband CPW fed antenna," *Wireless Pers. Commun.*, vol. 113, no. 2, pp. 961–975, Jul. 2020.

[17] A. H. Desai and T. Upadhyaya, "Dual-band transparent and non-transparent antennas for wireless application," *Int. J. Electron. Lett.*, vol. 8, no. 2, pp. 170–179, Apr. 2020.

[18] A. Desai, T. Upadhyaya, J. Patel, R. Patel, and M. Palandoken, "Flexible CPW fed transparent antenna for WLAN and sub-6 GHz 5G applications," *Microw. Opt. Technol. Lett.*, vol. 62, no. 5, pp. 2090–2103, May 2020.

[19] S. Azizi, L. Canale, S. Ahyoud, G. Zissis, and A. Asselman, "Design of transparent antenna for 5G wireless applications," *Proceedings*, vol. 63, no. 1, p. 54, Dec. 2020.

[20] J. Hautcoeur, L. Talbi, K. Hettak, and M. Nedil, "60 GHz optically transparent microstrip antenna made of meshed AuGL material," *IET Microw., Antennas Propag.*, vol. 8, no. 13, pp. 1091–1096, Oct. 2014.

[21] A. S. M. Sayem, R. B. V. B. Simorangkir, K. P. Esselle, and R. M. Hashmi, "Development of robust transparent conformal antennas based on conductive mesh-polymer composite for unobtrusive wearable applications," *IEEE Trans. Antennas Propag.*, vol. 67, no. 12, pp. 7216–7224, Dec. 2019.

[22] Y. Goliya, A. Rivadeneyra, J. F. Salmeron, A. Albrecht, J. Mock, M. Haider, J. Russer, B. Cruz, P. Eschlwech, E. Biebl, M. Becherer, and M. R. Bobinger, "Next generation antennas based on screen-printed and transparent silver nanowire films," *Adv. Opt. Mater.*, vol. 7, no. 21, Nov. 2019, Art. no. 1900995.

[23] T. Jang, C. Zhang, H. Youn, J. Zhou, and L. J. Guo, "Semitransparent and flexible mechanically reconfigurable electrically small antennas based on tortuous metallic micromesh," *IEEE Trans. Antennas Propag.*, vol. 65, no. 1, pp. 150–158, Jan. 2017.

[24] J. Park, S. Y. Lee, J. Kim, D. Park, W. Choi, and W. Hong, "An optically invisible antenna-on-display concept for millimeter-wave 5G cellular devices," *IEEE Trans. Antennas Propag.*, vol. 67, no. 5, pp. 2942–2952, May 2019.

[25] C. Ji, D. Liu, C. Zhang, and L. J. Guo, "Ultrathin-metal-film-based transparent electrodes with relative transmittance surpassing 100%," *Nature Commun.*, vol. 11, no. 1, pp. 1–8, Dec. 2020.

[26] C. Zhang, C. Ji, Y. Park, and L. J. Guo, "Thin-metal-film-based transparent conductors: Material preparation, optical design, and device applications," *Adv. Opt. Mater.*, vol. 9, no. 3, Feb. 2021, Art. no. 2001298.

[27] I. Lee and J.-L. Lee, "Transparent electrode of nanoscale metal film for optoelectronic devices," *J. Photon. Energy*, vol. 5, no. 1, May 2015, Art. no. 057609.

[28] Y. Kim, C. Lee, S. Hong, C. W. Jung, and Y. Kim, "Design of transparent multilayer film antenna for wireless communication," *Electron. Lett.*, vol. 51, no. 1, pp. 12–14, 2015.

[29] S. Hong, S. H. Kang, Y. Kim, and C. W. Jung, "Transparent and flexible antenna for wearable glasses applications," *IEEE Trans. Antennas Propag.*, vol. 64, no. 7, pp. 2797–2804, Jul. 2016.

[30] S. Hong, Y. Kim, and C. W. Jung, "Transparent microstrip patch antennas with multilayer and metal-mesh films," *IEEE Antennas Wireless Propag. Lett.*, vol. 16, pp. 772–775, 2016.
[31] S. Hong, Y. Kim, and C. W. Jung, "Transparent UWB antenna with IZTO/Ag/IZTO multilayer electrode film," *Int. J. Antennas Propag.*, vol. 2016, pp. 1–8, Oct. 2016.
[32] J. Hautcoeur, F. Colombel, M. Himdi, and E. Cruz, "Radiofrequency performances of transparent ultra-wideband antennas," *Prog. Electromagn. Res. C*, vol. 22, pp. 259–271, 2011.
[33] J. Yun, "Ultrathin metal films for transparent electrodes of flexible optoelectronic devices," *Adv. Funct. Mater.*, vol. 27, no. 18, May 2017, Art. no. 1606641.
[34] B. Levin, "Flat transparent antennas," *URSI Radio Sci. Bull.*, vol. 2016, no. 356, pp. 32–40, Mar. 2016.
[35] H. Saotome, S. Oi, and S. Akimoto, "Contactless measurement of sheet resistance using impulse voltage," *IEEE Trans. Magn.*, vol. 47, no. 10, pp. 2581–2583, Oct. 2011.
[36] S. P. Harvey, J. Moseley, A. Norman, A. Stokes, B. Gorman, P. Hacke, S. Johnston, and M. Al-Jassim, "Investigating PID shunting in polycrystalline silicon modules via multiscale, multitechnique characterization," *Prog. Photovolt., Res. Appl.*, vol. 26, no. 6, pp. 377–384, Jun. 2018.
[37] A. Klöppel, W. Kriegseis, B. K. Meyer, A. Scharmann, C. Daube, J. Stollenwerk, and J. Trube, "Dependence of the electrical and optical behaviour of ITO–silver–ITO multilayers on the silver properties," *Thin Solid Films*, vol. 365, no. 1, pp. 139–146, Apr. 2000.
[38] Y.-S. Park, K.-H. Choi, and H.-K. Kim, "Room temperature flexible and transparent ITO/Ag/ITO electrode grown on flexile PES substrate by continuous roll-to-roll sputtering for flexible organic photovoltaics," *J. Phys. D, Appl. Phys.*, vol. 42, no. 23, Dec. 2009, Art. no. 235109.
[39] K.-H. Choi, H.-J. Nam, J.-A. Jeong, S.-W. Cho, H.-K. Kim, J.-W. Kang, D.-G. Kim, and W.-J. Cho, "Highly flexible and transparent $InZnSnO_x$/Ag/$InZnSnO_x$ multilayer electrode for flexible organic light emitting diodes," *Appl. Phys. Lett.*, vol. 92, no. 22, p. 194, 2008.
[40] J.-A. Jeong, Y.-S. Park, and H.-K. Kim, "Comparison of electrical, optical, structural, and interface properties of IZO-Ag-IZO and IZO-Au-IZO multilayer electrodes for organic photovoltaics," *J. Appl. Phys.*, vol. 107, no. 2, Jan. 2010, Art. no. 023111.
[41] M. Sawada, M. Higuchi, S. Kondo, and H. Saka, "Characteristics of indium-tin-oxide/silver/indium-tin-oxide sandwich films and their application to simple-matrix liquid-crystal displays," *Jpn. J. Appl. Phys.* vol. 40, no. 5R, p. 3332, 2001.
[42] Y. S. Jung, Y. W. Choi, H. C. Lee, and D. W. Lee, "Effects of thermal treatment on the electrical and optical properties of silver-based indium tin oxide/metal/indium tin oxide structures," *Thin Solid Films*, vol. 440, nos. 1–2, pp. 278–284, Sep. 2003.
[43] J.-A. Jeong and H.-K. Kim, "Low resistance and highly transparent ITO–Ag–ITO multilayer electrode using surface plasmon resonance of ag layer for bulk-heterojunction organic solar cells," *Sol. Energy Mater. Sol. Cells*, vol. 93, no. 10, pp. 1801–1809, Oct. 2009.
[44] N. Ren, J. Zhu, and S. Ban, "Highly transparent conductive ITO/Ag/ITO trilayer films deposited by RF sputtering at room temperature," *AIP Adv.*, vol. 7, no. 5, May 2017, Art. no. 055009.
[45] E. F. Schubert, "Human eye sensitivity and photometric quantities," in *Light-Emitting Diodes*. New York, NY, USA: Cambridge Univ. Press, 2006, pp. 275–291.
[46] A. Dhar and T. L. Alford, "High quality transparent TiO_2/Ag/TiO_2 composite electrode films deposited on flexible substrate at room temperature by sputtering," *APL Mater.*, vol. 1, no. 1, Jul. 2013, Art. no. 012102.

JEONG-WOOK KIM received the B.S. degree in electronic engineering from Pusan National University, Busan, South Korea, in 2018, and the M.S. degree in electrical engineering from the Korea Advanced Institute of Science and Technology (KAIST), where he is currently pursuing the Ph.D. degree in electrical engineering. His current research interests include wireless power charging systems, phased array antenna systems, vehicle invisible antenna, RADAR systems, and signal processing.

JU-IK OH received the B.S. degree in electronic engineering from Inha University, Incheon, Republic of Korea, in 2017, and the M.S. degree in electrical engineering from the Korea Advanced Institute of Science and Technology (KAIST), Daejeon, Republic of Korea, in 2019, where he is currently pursuing the Ph.D. degree in electrical engineering. His current research interests include millimeter-wave antennas, RF front-end design, and antenna array systems.

KWANG-SEOK KIM received the B.S. degree from Soongsil University, Seoul, South Korea, in 2013, and the M.S. and Ph.D. degrees in electrical engineering from the Korea Advanced Institute of Science and Technology (KAIST), Daejeon, South Korea, in 2015 and 2021, respectively.

From 2015 to 2018, he worked at the Samsung Electronics Semiconductor Research and Development Center, Hwaseong-si, South Korea, where he analyzed signal integrity (SI), power integrity (PI), and electromagnetic interference/electromagnetic compatibility (EMI/EMC) for high-speed memory package and systems. Since 2021, he has been a Senior Researcher with the Affiliated Research Organization of the Electronics and Telecommunications Research Institute, Daejeon. His research interests include electromagnetic topology (EMT), electromagnetic pulse (EMP), partial discharge (PD), defect diagnostic techniques, EM analysis techniques, SI, PI, EMI/EMC, RF system applications, and phased array antenna systems.

JONG-WON YU (Member, IEEE) received the B.S., M.S., and Ph.D. degrees in electrical engineering from the Korea Advanced Institute of Science and Technology (KAIST), Daejeon, South Korea, in 1992, 1994, and 1998, respectively. From 2000 to 2001 and 2001 to 2004, he was also with Wide Telcom Head and Telson, South Korea. From 2004 to 2013, he was with KAIST, initially as an Assistant Professor of electrical engineering and as an Associate Professor. He is currently a Professor at KAIST. His research interests include microwave/millimeter-wave circuits (monolithic microwave integrated circuits (MMICs), and hybrid), wireless communication systems, and RFID/ubiquitous sensor networks.

KANG-JAE JUNG received the B.S. degree in electronic engineering from Kangnam University, Gyeonggi-do, South Korea, in 2002, and the M.S. and Ph.D. degrees in radio sciences and engineering from Kwangwoon University, Seoul, South Korea, in 2004 and 2009, respectively. He is currently working as a Research Fellow at LG Electronics. His research interests include mobile antennas, invisible antennas, and wireless communication systems.

IL-NAM CHO received the B.S. degree in electronic engineering from Kookmin University, Seoul, South Korea, in 1994, and the M.S. degree in electrical and electronic engineering from Yonsei University, Seoul, in 2009. He is currently a Research Fellow at LG Electronics. His research interests include invisible antennas, millimeter-wave antennas, and wireless communication systems.